

# LoaQ: Layer-wise Output Approximation Quantization

Li Lin<sup>1</sup>, Xiaojun Wan<sup>1</sup>

<sup>1</sup>Wangxuan Institute of Computer Technology, Peking University  
efsotr.l@stu.pku.edu.cn, wanxiaojun@pku.edu.cn

## Abstract

A natural and intuitive idea in model quantization is to approximate each component’s quantized output to match its original. Layer-wise post-training quantization (PTQ), though based on this idea, adopts a strictly local view and can achieve, at best, only activation-aware approximations of weights. As a result, it often leads to insufficient approximations and practical deviations from this guiding intuition. Recent work has achieved a more accurate approximation of linear-layer outputs within the framework of layer-wise PTQ, but such refinements remain inadequate for achieving alignment with the full model output. Based on a deeper understanding of the structural characteristics of mainstream LLMs, we propose **LoaQ**, an output-approximation method for layer-wise PTQ that explicitly targets output-level consistency. It better aligns with this intuition and can feature a simple closed-form solution, making it orthogonal to existing techniques and readily integrable into existing quantization pipelines. Experiments on the LLaMA and Qwen model families demonstrate that LoaQ performs effectively in both weight-only and weight-activation joint quantization. By integrating seamlessly with existing quantization strategies, it further enhances overall quantization quality and shows strong potential to advance the frontier of post-training quantization.

## 1 Introduction

In recent years, large-scale models have achieved remarkable breakthroughs in performance, yet these advances come with significant memory overhead, posing challenges for practical deployment. Model compression techniques (Zhu et al. 2024) have emerged as a promising solution to this problem, with post-training quantization (PTQ) (Krishnamoorthi 2018) being one of the most impactful approaches. Within PTQ methods, layer-wise PTQ has attracted particular attention. By formulating quantization at the level of individual linear layers, layer-wise PTQ simplifies both the process and the associated optimization objectives. Despite this simplification, layer-wise PTQ consistently delivers strong empirical performance. Moreover, this approach offers significant efficiency advantages: it can quantize large-scale models within a short time using only a single GPU. Beyond its standalone effectiveness, layer-wise PTQ also serves as an excellent initialization for end-to-end PTQ frameworks, accelerating their convergence and

thereby further enhancing the final model’s performance. These properties collectively make layer-wise PTQ an important contributor to advancing the performance boundaries of quantized models.

Although layer-wise PTQ methods, ranging from the classic GPTQ (Frantar et al. 2023) to the more recent MagR (Zhang et al. 2024), have achieved notable success, they still predominantly focus on weight approximation. This focus exposes a fundamental limitation: to maintain their layer-wise nature, these methods typically depend only on the input to each linear layer. Consequently, they are confined to activation-aware weight approximation, which diverges from the natural objective of output approximation. Recent approaches, including GPTAQ (Li et al. 2025), Qronos (Zhang et al. 2025), and QEP (Arai and Ichikawa 2025), overcome this limitation through an error-compensation strategy. Specifically, they modify weights to compensate for the mismatch between pre- and post-quantization inputs, while still following the forward layer-wise quantization sequence. By explicitly incorporating this compensation, these methods enable a more output-oriented optimization at the level of individual linear layers and ultimately achieve more accurate linear-layer output approximation.

While previous methods approximate outputs at the linear-layer level, this scope remains confined and fails to account for residual connections and RMSNorm, making it insufficient for model-level output approximation. To address these issues, we extend our perspective to the sub-layer level, allowing us to naturally account for these components. Building on this idea, we introduce LoaQ, a layer-wise PTQ method that explicitly targets sub-layer output approximation, thereby overcoming the limitations of linear-layer methods and aligning more closely with model-level output approximation. Extensive experiments on LLaMA (Touvron et al. 2023; Grattafiori et al. 2024) and Qwen (Yang et al. 2025) model families confirm that LoaQ consistently preserves high quantization accuracy across diverse tasks and quantization settings. Furthermore, LoaQ integrates seamlessly with other quantization strategies, including the Hadamard transform and NeUQI (Lin, Hu, and Wan 2025), and delivers additional improvements in overall model performance. Code and models will be released.

Our main contributions are as follows:

- We present a perspective based on output approximation and analyze the characteristics of the resulting errors, thereby offering potential directions for designing more effective quantization strategies.
- We propose LoaQ, a novel approach that effectively addresses the output approximation problem within the layer-wise PTQ framework.
- We validate the strong performance and potential of LoaQ through extensive experiments on diverse tasks and quantization settings, advancing the performance limits of post-training quantization, particularly for layer-wise methods.

## 2 Preliminaries

### 2.1 Notation

In this section, we introduce the notation used consistently throughout this paper.

Let  $W, Q \in \mathbb{R}^{N \times M}$  denote the original and quantized weight matrices, respectively. Similarly, let  $X \in \mathbb{R}^{T \times N}$  and  $\hat{X} \in \mathbb{R}^{T \times N}$  represent the activation matrices before and after quantization, where variables with a hat (e.g.,  $\hat{X}$ ) indicate quantized versions of their unhat counterparts (e.g.,  $X$ ). Here,  $T$  is the number of tokens, and  $N$  and  $M$  are the input and output feature dimensions, respectively.

We define the following  $N \times N$  matrices that arise in the layer-wise quantization loss:  $H = \hat{X}^\top \hat{X}$ , representing the Hessian matrix of quantization loss;  $C = \hat{X}^\top (X - \hat{X})$ , representing the error compensation matrix; and  $I = I_N$ , the  $N \times N$  identity matrix.

For a vector  $x \in \mathbb{R}^N$ , define the normalized vector as

$$\text{Norm}(x) = r(x) \cdot x, \quad (1)$$

where  $r(x) = (N^{-1} \sum_i x_i^2 + \epsilon)^{-1/2}$ , with  $\epsilon > 0$  added for numerical stability.

For a matrix  $X \in \mathbb{R}^{T \times N}$ , define the row-wise normalized matrix as

$$\text{Norm}(X) = R(X)X, \quad (2)$$

where  $R(X) = \text{diag}(r(X_{1,:}), \dots, r(X_{T,:}))$ .

### 2.2 Layer-wise PTQ

In model quantization, a common assumption is that accurately approximating the weights of each linear layer is sufficient to maintain overall model performance. Layer-wise PTQ builds on this principle by treating the quantization of each linear layer as an independent optimization task. To enhance efficiency, it employs a single-pass strategy that sequentially quantizes layers during one forward pass. Under this design, the GPU stores solely the minimal data necessary for the active layer, typically retaining only the post-quantization input for the optimization process. This approach substantially reduces computational overhead and memory consumption, resulting in a streamlined and efficient layer-wise PTQ framework.

In the weight-only quantization setting of layer-wise PTQ, most classical weight approximation objectives fall into two main forms.

### 1. Direct weight approximation minimizes

$$\arg \min_Q \|Q - W\|_F^2, \quad (3)$$

where the objective seeks the optimal quantized value for each weight individually. A representative method under this formulation is Round-To-Nearest (RTN), which quantizes each weight by rounding it to the nearest value in the quantization grid.

### 2. Activation-aware weight approximation minimizes

$$\arg \min_Q \|\hat{X}(Q - W)\|_F^2, \quad (4)$$

where the objective explicitly incorporates the input activation distribution, thereby mitigating the impact of quantization error on the linear layer output. A typical approach in this category is GPTQ, which leverages second-order information of this approximation objective to further reduce output distortion during quantization.

In joint weight and activation quantization, researchers have explored several strategies that vary in complexity and optimization scope: (i) independently quantizing weights and activations, following the principle of direct weight approximation; (ii) quantizing activations first, followed by activation-aware weight approximation to optimize the weights; (iii) jointly optimizing both weight and activation quantization to directly minimize the overall output error, which is often carried out based on the results of (i) or (ii).

Layer-wise PTQ can be further enhanced by integrating various complementary techniques. Notable examples include SmoothQuant (Xiao et al. 2023), which balances the numerical scales of weights and activations to alleviate quantization error; Hadamard transform, used in QuaRot (Ashkboos et al. 2024) and QuIP# (Chee et al. 2023), applies a Hadamard transformation to smooth the weight distribution and reduce quantization error; NeUQI (Lin, Hu, and Wan 2025), which improves the initialization of uniform quantization parameters; and BCD (Nair and Suggala 2024), which employs coordinate descent to refine the quantized weight of each linear layer.

### 2.3 Sub-layer

In mainstream LLM architectures, each Transformer layer consists of a self-attention sub-layer and an MLP sub-layer. As shown in Figure 1, each sub-layer typically includes an RMSNorm, a sub-layer module, and a residual connection adding the input to the output. The sub-layer module can be uniformly represented in a simplified form:

$$X_k^{\text{out}} = \phi(\text{Norm}(h_k)W_{\text{in}}), \quad (5)$$

$$h_{k+1} = h_k + X_k^{\text{out}}W_{\text{out}}. \quad (6)$$

In this formulation:

- For the self-attention module,  $W_{\text{in}} = [W_q; W_k; W_v]$  are the input projections to queries, keys, and values. The nonlinearity  $\phi$  denotes the masked attention mechanism, which typically includes QK-normalization (if applicable), rotary positional encoding (RoPE), and causal attention over the resulting representations. The output projection is given by  $W_{\text{out}} = W_o$ .

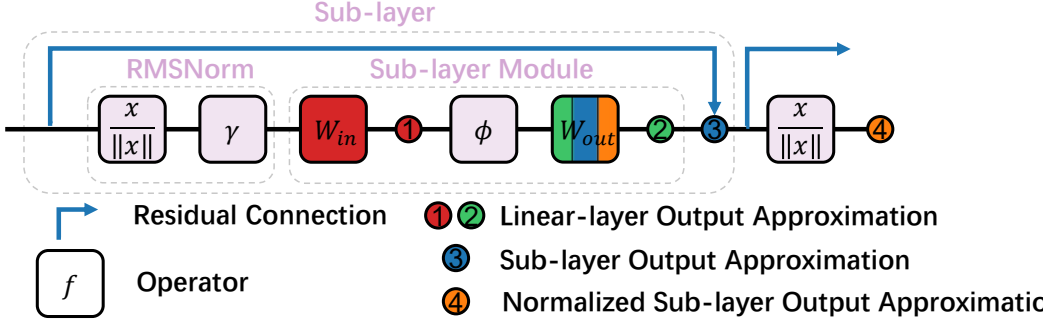


Figure 1: The overall diagram of **LoaQ**. Each colored circle denotes an intermediate result, which LoaQ aims to approximate when quantizing the weight matrix of the corresponding color. The red circle 1 and green circle 2 correspond to the parts approximated by Linear-layer Output Approximation, the blue circle 3 corresponds to Sub-layer Output Approximation, and the orange circle 4 corresponds to Normalized Sub-layer Output Approximation.

- For the MLP module,  $W_{\text{in}} = [W_{\text{gate}}; W_{\text{up}}]$  corresponds to the projections used in the gated feedforward path. The nonlinearity  $\phi$  denotes an elementwise activation that gates the  $W_{\text{up}}$  projection using  $W_{\text{gate}}$  in the expanded hidden space. The projection back to the model dimension is given by  $W_{\text{out}} = W_{\text{down}}$ .

### 3 Methodology

In this section, we introduce **LoaQ**, short for Layer-wise Output Approximation Quantization. LoaQ builds on the layer-wise post-training quantization framework, which typically focuses on quantizing only  $W_{\text{in}}$  and  $W_{\text{out}}$ . Extending this framework, LoaQ incorporates additional factors during quantization to achieve more accurate approximations. As shown in Figure 1, LoaQ consists of three components that progressively target the true output approximation with increasing accuracy: linear-layer, sub-layer, and sub-layer followed by RMSNorm. In contrast, GPTAQ and Qronos only target the linear-layer part. Each component in LoaQ builds upon the previous one, achieving increasingly accurate approximations by strategically selecting intermediate results within the model. The intermediate results highlighted by the red circle 1 and green circle 2 correspond to the linear-layer outputs, which are approximated using the method detailed in Section 3.1. With deeper insights into LLM architectures, the approach applied to the blue circle 3 replaces the approximation at the green circle 2 and is further enhanced by the method associated with the orange circle 4.

#### 3.1 Linear Layer Output Approximation

In this subsection, we aim to make the results at the red circle 1 and the green circle 2 in Figure 1 after quantization closely match their pre-quantization counterparts by approximating the outputs of the corresponding linear layers. For each linear layer, this leads to the following optimization objective.

$$\arg \min_Q \|\hat{X}Q - XW\|_F^2. \quad (7)$$

Through a series of equivalent transformations, detailed in Appendix A, this is equivalent to:

$$\arg \min_Q \|\hat{X}(Q - (I + H^{-1}C)W)\|_F^2. \quad (8)$$

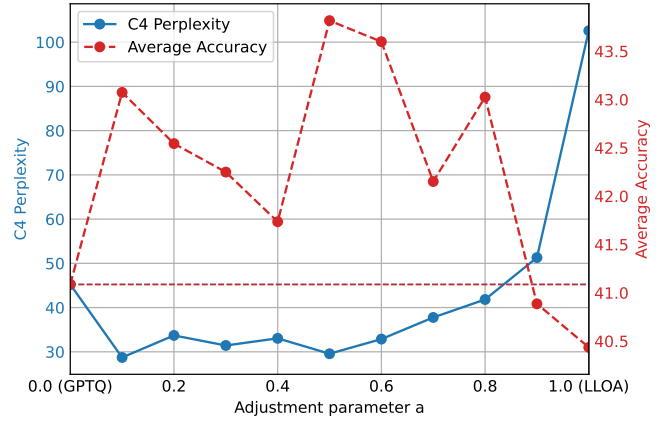


Figure 2: LLaMA 3.2 1B performance under different values of the adjustment parameter  $\alpha$  with 3-bit channel-wise quantization.

Therefore, updating  $W$  to  $(I + H^{-1}C)W$  adapts the problem to the activation-aware framework, allowing direct use of existing activation-aware weight approximation methods.

Preliminary experiments on LLaMA 3.2 1B with 3-bit channel-wise quantization show that directly adding the linear-layer output approximation on top of the original GPTQ method leads to performance degradation, as demonstrated by the comparison between GPTQ and the Linear-Layer Output Approximation (LLOA) in Figure 2. Interestingly, for other methods based on linear-layer output approximations, such as GPTAQ and Qronos, we also observe similar degradation when they are applied solely to quantize the linear layers on top of the original layer-wise PTQ methods. To address this, upon careful examination of the code, we found that these methods employ different strategies to mitigate the risk of large deviations. For instance, GPTAQ defines its objective as a weighted combination of the linear-layer output approximation objective and the original objective. Qronos, in contrast, resets the accumulated error at the start of each Transformer layer and focuses only on the newly introduced error within that layer. These strategies help ensure that the

approximation target remains closely aligned with the true optimization objective.

Consequently, we adopt a more general technique by introducing a tunable adjustment parameter  $\alpha \in [0, 1]$ , modifying the update rule to  $W \leftarrow (I + \alpha H^{-1}C)W$ . Figure 2, LLOA is indeed effective, but when the correction is too strong, it can deviate excessively from the final optimization objective.

QEP attributes this phenomenon to overfitting on the calibration set, as the number of calibration tokens is not much larger than the hidden state dimension. We instead identify a different cause. Although aligning linear-layer outputs with a surrogate objective is formally consistent with the final goal, residual errors can persist even under ideal conditions. Moreover, the surrogate objective may fail to capture the true problem structure, producing solutions that deviate from the real optimum and occasionally degrading performance under the final metric. These findings reveal the limitations of relying solely on such alignment constraints and naturally lead to the question of what in the LLM structure better represents the true optimization objective. Addressing this question is the focus of the following two sections.

### 3.2 Sub-layer Output Approximation

In this subsection, we shift the focus from approximating the green circle 2 to approximating the blue circle 3 in Figure 1, aiming to make the post-quantization results closely match their pre-quantization counterparts by aligning the outputs of the corresponding sub-layer.

Ideally, methods that approximate only the linear-layer output can at best match the output of the sub-layer module but fail to approximate the full sub-layer output  $h_{k+1}$ . This limitation arises because, by neglecting the residual connection, these methods overlook the accumulated errors propagated through the residual stream. In our approach, we aim to match the sub-layer output while preserving the layer-wise property. To this end, the sub-layer output approximation is only considered when quantizing  $W_{\text{out}}$ . That is, we aim to approximate  $h_{k+1} = h_k + X_k^{\text{out}}W$  by  $\hat{h}_k + \hat{X}_k^{\text{out}}Q$ . Accordingly, for notational simplicity, we omit both the subscript  $k$  and the superscript out in the following formulation, and write the optimization objective as:

$$\arg \min_Q \|\hat{h} + \hat{X}Q - (h + XW)\|_F^2 \quad (9)$$

By transformation, we obtain the following equivalent form:

$$\begin{aligned} \arg \min_Q \|\hat{X}(Q - ((I + H^{-1}C)W + \\ H^{-1}\hat{X}^\top(h - \hat{h})))\|_F^2, \end{aligned} \quad (10)$$

whose equivalence is proven in Appendix A. Updating  $W$  to  $(I + H^{-1}C)W + H^{-1}\hat{X}^\top(h - \hat{h})$  essentially reformulates the objective into a classical activation-aware weight approximation, and thus it can be solved using the same methodology. Since this might still not perfectly align with the true optimization objective and can lead to large deviations, we further introduce a tunable adjustment parameter  $\beta$  and modify the update rule to:  $W \leftarrow (I + \alpha H^{-1}C)W + \beta H^{-1}\hat{X}^\top(h - \hat{h})$ , where  $\alpha, \beta \in [0, 1]$  control the relative influence of the two components.

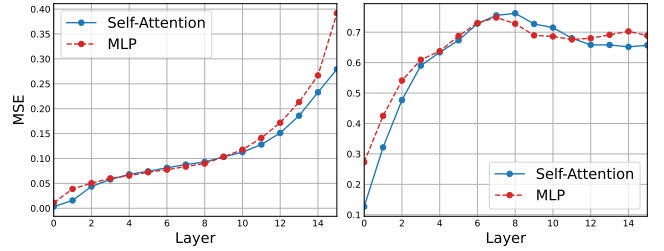


Figure 3: Results under 3-bit quantization on LLaMA 3.2 1B, showing the mean squared error (MSE) of sub-layers' outputs without outlier tokens. The left plot shows the MSE of unnormalized outputs, and the right plot shows the MSE of normalized outputs.

### 3.3 Normalized Sub-layer Output Approximation

In this subsection, we shift the focus from approximating the blue circle 3 to approximating the orange circle 4 in Figure 1, aiming to make the post-quantization results closely match their pre-quantization counterparts by approximating the normalized outputs of the corresponding sub-layer.

Based on the above understanding of the Transformer architecture, the presence of residual connections leads to the accumulation of quantization error as the depth increases, as shown in the left plot of Figure 3. This raises the question of how the model remains stable despite the accumulation of quantization error. Upon closer examination, we observed that an RMSNorm layer is consistently applied before the input to each sub-layer module and the final language model head. As illustrated in the right plot of Figure 3, this normalization mechanism prevents the mean squared error (MSE) between normalized outputs from growing beyond a certain depth.

Since a normalization layer follows each sub-layer, it is the normalized output rather than the raw sub-layer output that directly influences subsequent linear projections. As such, aligning the normalized outputs of the quantized and original models becomes critical for maintaining the model's functional integrity. To address this, we refine the objective to explicitly target the normalized sub-layer outputs:

$$\arg \min_Q \|\text{Norm}(\hat{h} + \hat{X}Q) - \text{Norm}(h + XW)\|_F^2 \quad (11)$$

To simplify the expression, we write the normalization term as  $\text{Norm}(\hat{h} + \hat{X}Q) = R(\hat{h} + \hat{X}Q)(\hat{h} + \hat{X}Q)$ , where both the scaling function  $R(\cdot)$  and the input contain the quantized parameter  $Q$ . To reduce the number of unknowns and decouple the quantized terms, we replace  $Q$  with the original weight  $W$  inside the scaling function  $R(\cdot)$ , and can then be transformed into the form:

$$\begin{aligned} \arg \min_Q \& \|(R(\hat{h} + \hat{X}W)\hat{h} + (R(\hat{h} + \hat{X}W)\hat{X})Q) \\ & - (R(h + XW)h + (R(h + XW)X)W)\|_F^2 \end{aligned} \quad (12)$$

This yields the same form as objective (9), allowing us to apply the same solution.

Model	Size	Method	Wiki2↓	C4↓	ArcC↑	ArcE↑	HellaS↑	PiQA↑	WinoG↑	Acc↑
7B	LLaMA 2	GPTQ	6875	2237	<b>22.27</b>	25.25	26.02	53.10	50.91	35.51
		GPTAQ	1269	246	21.76	26.89	25.74	53.32	47.12	34.97
		Qronos	1505	306	20.65	27.82	25.96	53.70	49.09	35.44
		LoaQ	<b>214</b>	<b>67.31</b>	19.45	<b>30.56</b>	<b>28.71</b>	<b>55.98</b>	<b>54.46</b>	<b>37.83</b>
13B	LLaMA 2	GPTQ	4235	580	<b>20.90</b>	25.84	25.72	50.33	50.91	34.74
		GPTAQ	145	62.05	20.56	26.89	26.99	53.43	<b>51.85</b>	35.95
		Qronos	352	110	20.82	26.68	26.78	52.18	50.12	35.31
		LoaQ	<b>111</b>	<b>47.26</b>	20.14	<b>33.54</b>	<b>31.61</b>	<b>59.52</b>	50.75	<b>39.11</b>
70B	LLaMA 2	GPTQ	71.05	40.17	<b>21.59</b>	28.03	26.96	53.48	53.12	36.63
		GPTAQ	<b>40.09</b>	28.37	<b>21.59</b>	28.91	28.98	54.08	51.46	37.00
		Qronos	66.52	41.75	19.45	34.85	29.78	60.23	53.04	39.47
		LoaQ	41.62	<b>28.03</b>	19.97	<b>35.98</b>	<b>32.53</b>	<b>60.88</b>	<b>54.85</b>	<b>40.84</b>
8B	LLaMA 3	GPTQ	>1e4	>1e4	22.01	25.04	25.87	<b>54.62</b>	48.15	35.14
		GPTAQ	>1e4	4409	20.99	<b>25.29</b>	25.88	52.99	48.46	34.72
		Qronos	>1e4	>1e4	<b>22.95</b>	25.21	25.59	54.35	48.62	35.35
		LoaQ	<b>5497</b>	<b>528</b>	22.53	24.41	<b>26.37</b>	53.05	<b>51.54</b>	<b>35.58</b>
70B	LLaMA 3	GPTQ	>1e4	>1e4	21.25	25.17	25.72	52.34	51.14	35.12
		GPTAQ	>1e4	>1e4	22.70	24.87	<b>25.78</b>	53.21	51.22	35.56
		Qronos	<b>12147</b>	<b>9187</b>	20.22	25.17	25.73	53.10	49.80	34.81
		LoaQ	>1e4	>1e4	<b>23.21</b>	<b>26.39</b>	25.75	<b>53.32</b>	<b>52.41</b>	<b>36.22</b>
8B	Qwen 3	GPTQ	7151	2969	20.82	25.42	25.25	50.54	51.22	34.65
		GPTAQ	500	171	<b>21.16</b>	25.29	25.14	50.82	47.04	33.89
		Qronos	263	129	19.97	27.90	27.01	54.68	47.83	35.48
		LoaQ	<b>171</b>	<b>82.90</b>	18.52	<b>33.75</b>	<b>29.96</b>	<b>58.65</b>	<b>52.33</b>	<b>38.64</b>
14B	Qwen 3	GPTQ	1916	888	<b>23.46</b>	24.79	25.07	51.36	47.83	34.50
		GPTAQ	224	101	21.67	25.13	25.81	48.69	48.93	34.05
		Qronos	141	76.67	19.28	32.32	28.52	57.40	51.07	37.72
		LoaQ	<b>85.40</b>	<b>54.57</b>	21.08	<b>36.41</b>	<b>32.47</b>	<b>60.72</b>	<b>53.35</b>	<b>40.81</b>
32B	Qwen 3	GPTQ	8444	2843	21.67	24.75	25.61	51.90	49.57	34.70
		GPTAQ	321	117	<b>23.55</b>	24.07	26.62	50.38	51.14	35.15
		Qronos	156	77.23	23.46	28.11	29.63	54.13	48.86	36.84
		LoaQ	<b>107</b>	<b>60.44</b>	19.88	<b>34.43</b>	<b>33.33</b>	<b>60.45</b>	<b>52.25</b>	<b>40.07</b>

Table 1: Perplexity on Wiki2 and C4, along with the average zero-shot accuracy across five benchmarks (reported as **Acc**), for various quantized models using 2-bit channel-wise quantization. The arrows ↑/↓ indicate whether higher or lower is better.

## 4 Experiment

### 4.1 Baselines and Evaluation

We experiment with our proposed LoaQ on three commonly-used LLM families, covering different sizes: LLaMA 2 (7B, 13B, 70B) (Touvron et al. 2023), LLaMA 3 (8B, 70B) (Grattafiori et al. 2024) and Qwen 3 (8B, 14B, 32B) (Yang et al. 2025). Under the weight-only quantization setting, we compare LoaQ with the baseline GPTQ (Frantar et al. 2023) and two error compensation methods, Qronos (Zhang et al. 2025) and GPTAQ (Li et al. 2025). We also evaluate scenarios that incorporate effective quantization techniques such as NeUQI (Lin, Hu, and Wan 2025) and the Hadamard transform, in order to test whether LoaQ remains effective under these enhancements. In addition, LoaQ is assessed under the weight-activation quantization setting. A brief introduction to these techniques is provided in Appendix B. Following the previous work, all the quantized models are evaluated by measuring perplexity on the WikiText2 (**Wiki2**) (Merity et al.

2017) and **C4** (Raffel et al. 2020) validation sets, and zero-shot accuracy on five benchmarks: ARC-easy (**ArcE**), ARC-challenge (**ArcC**) (Clark et al. 2018), **PiQA** (Bisk et al. 2020), HellaSwag (**HellaS**) (Zellers et al. 2019), and Wino-Grande (**WinoG**) (Sakaguchi et al. 2021).

### 4.2 Implementation Detail

For weight-only quantization, we evaluate the 2-bit setting and the 3-bit setting, both using channel-wise quantization for weights. For weight-activation quantization, we adopt the W4A4 setting, where weights are quantized to 4 bits channel-wise and activations to 4 bits token-wise dynamically, with quantization parameters determined by the Min-Max method (Jacob et al. 2017). During calibration, we draw 128 samples of 2048 tokens each from the C4 dataset for LLaMA 2 and 3, and Qwen 3 families, whereas other studies may use WikiText2. We perform a hyperparameter grid search on LLaMA 3.2 1B and Qwen 3 1.7B, where  $\alpha$  ranges from 0 to 1 in increments of 0.1 and  $\beta$  ranges from 0 to 1 in increments of 0.05, and transfer the optimi-

Method	Wiki2↓	C4↓	Acc↑	Wiki2↓	C4↓	Acc↑
	2-bit			3-bit		
LLaMA 2 7B						
GPTQ	759	277	34.95	7.36	9.04	59.68
GPTAQ	64.88	39.36	37.14	6.93	8.54	60.35
Qronos	77.19	48.52	37.05	6.88	8.46	60.22
LoaQ	<b>44.65</b>	<b>23.76</b>	<b>41.81</b>	<b>6.73</b>	<b>8.31</b>	<b>60.91</b>
LLaMA 3 8B						
GPTQ	7883	1809	35.34	12.62	14.36	57.44
GPTAQ	175	94.41	35.20	9.57	12.85	60.24
Qronos	129	85.50	35.11	9.71	12.77	60.56
LoaQ	<b>83.79</b>	<b>49.43</b>	<b>38.35</b>	<b>9.30</b>	<b>12.56</b>	<b>61.52</b>
Qwen 3 8B						
GPTQ	2592	997	35.05	12.32	15.53	59.42
GPTAQ	103	59.24	35.22	12.13	15.35	59.59
Qronos	106	51.08	36.08	<b>11.89</b>	<b>15.19</b>	60.18
LoaQ	<b>45.45</b>	<b>33.53</b>	<b>41.26</b>	12.05	15.27	<b>62.25</b>

Table 2: Results on LLaMA 2 7B, LLaMA 3 8B, and Qwen 3 8B for 2-bit and 3-bit channel-wise quantization with the Hadamard transform.

mized configurations to the larger models. Additional tuning on larger models is conducted only when the transferred settings perform poorly. All experiments are conducted on a single NVIDIA A40 GPU. More implementation details are provided in Appendix C.

### 4.3 Main Result

Under the highly challenging 2-bit channel-wise quantization scenario, LoaQ generally surpasses the baseline GPTQ and two strong counterparts, GPTAQ and Qronos, as shown in Table 1. For LLaMA 3 70B, all methods perform poorly due to its inherent difficulty in 2-bit quantization. In contrast, LoaQ demonstrates strong and consistent performance across different model families and sizes.

As the bit-width increases, the performance gap between methods narrows, as shown in Table 1 of Appendix D. LoaQ continues to show clear advantages under the 3-bit setting, demonstrating robustness across model architectures, while in some cases performing on par with others and still offering slight benefits in specific scenarios.

### 4.4 Discussion

**Hadamard Transform** As shown in Table 2, we further evaluate LoaQ combined with the Hadamard transform, which smooths weight and activation distributions to mitigate quantization error. Compared with methods that focus only on linear-layer output approximation such as GPTAQ and Qronos, LoaQ substantially delivers better performance across all models. In the challenging 2-bit setting it remains stable where other methods fail, and even on Qwen 3 8B under the 3-bit setting, where perplexities are relatively higher, it still achieves the best overall accuracy. These results highlight the robustness and wide applicability of LoaQ.

Method	Wiki2↓	C4↓	Acc↑	Wiki2↓	C4↓	Acc↑
	No Transform			Hadamard Trasform		
LLaMA 2 7B						
GPTQ	17.44	17.62	47.88	12.41	13.22	52.91
GPTAQ	13.91	14.33	49.36	9.63	10.75	54.79
Qronos	12.97	13.04	52.36	9.99	10.90	55.08
LoaQ	<b>11.10</b>	<b>11.47</b>	<b>53.21</b>	<b>8.62</b>	<b>9.82</b>	<b>56.44</b>
LLaMA 3 8B						
GPTQ	46.03	33.21	48.74	18.15	22.03	51.93
GPTAQ	43.34	27.84	50.69	16.21	18.48	53.88
Qronos	42.38	27.65	50.86	15.73	17.57	53.78
LoaQ	<b>28.88</b>	<b>22.87</b>	<b>52.24</b>	<b>12.43</b>	<b>15.34</b>	<b>55.51</b>
Qwen 3 8B						
GPTQ	64.02	36.12	42.55	17.15	19.74	59.64
GPTAQ	205	103	38.34	170	98.48	37.81
Qronos	50.54	31.44	48.27	16.06	18.94	58.10
LoaQ	<b>28.74</b>	<b>23.70</b>	<b>51.40</b>	<b>15.59</b>	<b>18.52</b>	<b>60.01</b>

Table 3: Results on LLaMA 2 7B, LLaMA 3 8B, and Qwen 3 8B for 2-bit channel-wise quantization with and without the Hadamard transform, combined with NeUQI.

**Parameter Initialization** We further evaluated LoaQ combined with NeUQI, an effective quantization parameter initialization method, and assessed its performance with and without the equally effective Hadamard transform, as shown in Table 3. Under the 2-bit channel-wise setting, LoaQ consistently outperforms GPTQ, GPTAQ, and Qronos, while under the 3-bit channel-wise setting, it achieves stable improvements. The results obtained through these combinations with effective quantization techniques highlight LoaQ’s strong potential to serve as an important component of an ultimate PTQ solution, particularly for layer-wise PTQ under low-bit-width configurations.

**Weight-Activation Quantization** For the W4A4 setting, as shown in Table 4, LoaQ remains highly competitive. Without the Hadamard transform, LoaQ demonstrates clear performance gains over a wide range of models. When the Hadamard transform is applied, GPTAQ and Qronos experience performance drops on some models, whereas LoaQ still delivers slight improvements. These results demonstrate that LoaQ is effective in both weight-only and weight-activation quantization, confirming its broad applicability to model quantization.

**Ablation Study** We further evaluate the individual contributions of the Sub-layer Output Approximation (SOA) and the Normalized Sub-layer Output Approximation (NOA) in LoaQ through an ablation study on LLaMA 2 7B under 2-bit channel-wise quantization. We examine three configurations: removing SOA, removing NOA, and removing both SOA and NOA. The results in Table 5 demonstrate that both SOA and NOA provide clear benefits. Moreover, as shown in Figure 4, the top two plots without the Hadamard transform reveal that SOA markedly reduces the mean squared error of hidden states across all layers, while NOA substantially low-

Method	Wiki2↓	C4↓	Acc↑	Wiki2↓	C4↓	Acc↑
	No Transform			Hadamard Trasform		
LLaMA 2 7B						
GPTQ	429	445	36.98	6.15	7.76	62.38
GPTAQ	902	617	35.65	6.20	7.73	61.93
Qronos	579	159	35.22	6.38	7.91	61.64
Ours	<b>62.98</b>	<b>31.06</b>	<b>39.33</b>	<b>6.11</b>	<b>7.65</b>	<b>62.47</b>
LLaMA 3 8B						
GPTQ	323	422	38.33	8.06	11.38	62.53
GPTAQ	52.08	50.59	44.16	<b>7.85</b>	<b>11.16</b>	63.38
Qronos	411	166	36.50	8.68	11.77	61.96
Ours	<b>28.38</b>	<b>30.76</b>	<b>45.09</b>	7.91	11.18	<b>63.99</b>
Qwen 3 8B						
GPTQ	2919	2241	34.72	<b>11.02</b>	<b>14.63</b>	63.57
GPTAQ	3380	2043	35.15	11.07	14.69	64.53
Qronos	1943	1158	35.12	12.16	15.73	64.78
Ours	<b>1187</b>	<b>643</b>	<b>35.38</b>	11.33	15.00	<b>65.31</b>

Table 4: Results of W4A4 with and without Hadamard Transform on LLaMA 2 7B, LLaMA 3 8B, and Qwen 3 8B.

Method	Wiki2↓	C4↓	Acc↑	Wiki2↓	C4↓	Acc↑
	No Transform			Hadamard Trasform		
LoaQ	<b>214</b>	<b>67.31</b>	<b>37.83</b>	44.65	23.76	<b>41.81</b>
-SOA	225	69.93	37.57	45.79	26.81	40.69
-NOA	1757	250	35.04	<b>36.50</b>	<b>23.12</b>	40.83
-SOA	328	95.15	35.85	44.00	28.32	40.06

Table 5: Ablation study of the SOA and NOA modules with and without the Hadamard Transform on LLaMA 2 7B using 2-bit channel-wise quantization.

ers errors in the early layers. The corrective effect of NOA appears to diminish with increasing layer depth, likely because accumulated quantization errors weaken its impact. In contrast, the bottom two plots with the Hadamard transform show a considerable overall improvement. Under this setting, the influence of NOA is less directly reflected in the error, while SOA still exhibits a clear reduction in errors. These results confirm that both SOA and NOA are effective, and their combination, especially when paired with the Hadamard transform, further enhances quantization performance.

**Quantization Overhead** The overhead, reported in minutes in Table 6, represents the time required to execute the quantization algorithms for 3-bit quantization of the Qwen 3 model family on an NVIDIA A40 GPU. LoaQ, along with GPTAQ and Qronos, needs to store and process both pre- and post-quantization inputs as well as auxiliary information, resulting in overheads of the same order of magnitude. Compared with GPTAQ and Qronos, LoaQ incurs a slightly higher cost because it leverages richer contextual information and performs additional computations at multiple stages of the quantization process. This modest increase in quanti-

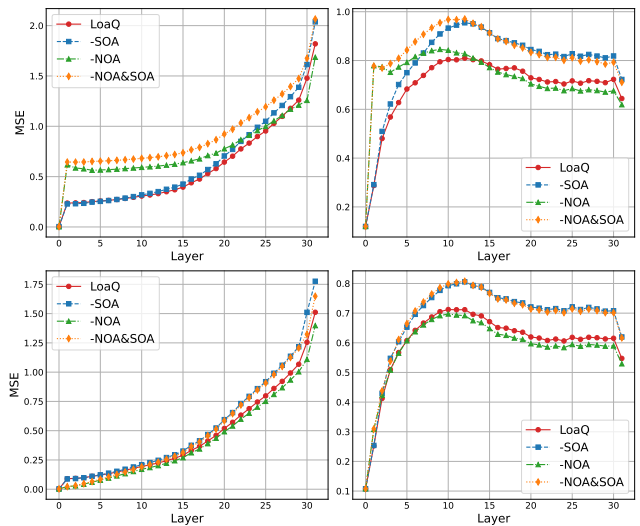


Figure 4: Results of 2-bit channel-wise quantization on LLaMA 2 7B, presenting the mean squared error (MSE) of Transformer layer outputs excluding outlier tokens. The top two plots show the MSE without the Hadamard transform, while the bottom two plots show the MSE with the Hadamard transform. For each row, the left plot corresponds to unnormalized outputs, and the right plot corresponds to normalized outputs.

Method	Size		
	8B	14B	32B
GPTQ	11.48	20.63	55.23
GPTAQ	17.92	34.13	100.00
Qronos	17.45	33.27	97.87
LoaQ	19.68	37.78	108.03

Table 6: Overhead in minutes of 3-bit channel-wise quantization on the Qwen 3 family using an NVIDIA A40 GPU.

zation time is well justified by the substantial performance improvements achieved by LoaQ, reflecting the effectiveness of its design.

## 5 Conclusion

Across various models, settings, and combinations with advanced quantization techniques, LoaQ consistently outperforms methods that rely solely on linear-layer output approximation, such as GPTAQ and Qronos. This demonstrates the value of designing layer-wise PTQ based on the structure of LLMs, leading to quantization methods that better align with optimization objectives. These results also underscore LoaQ’s potential to enhance the effectiveness of layer-wise PTQ. In future work, we plan to further explore techniques such as error compensation and output approximation, as well as investigate phenomena related to quantization errors, to develop more effective strategies for layer-wise PTQ.

## References

Arai, Y.; and Ichikawa, Y. 2025. Quantization Error Propagation: Revisiting Layer-Wise Post-Training Quantization. arXiv:2504.09629.

Ashkboos, S.; Mohtashami, A.; Croci, M.; Li, B.; Cameron, P.; Jaggi, M.; Alistarh, D.; Hoefer, T.; and Hensman, J. 2024. Quarot: Outlier-free 4-bit inference in rotated llms. *Advances in Neural Information Processing Systems*, 37: 100213–100240.

Bisk, Y.; Zellers, R.; Gao, J.; Choi, Y.; et al. 2020. Piqa: Reasoning about physical commonsense in natural language. In *Proceedings of the AAAI conference on artificial intelligence*, volume 34, 7432–7439.

Chee, J.; Cai, Y.; Kuleshov, V.; and De Sa, C. M. 2023. Quip: 2-bit quantization of large language models with guarantees. *Advances in Neural Information Processing Systems*, 36: 4396–4429.

Clark, P.; Cowhey, I.; Etzioni, O.; Khot, T.; Sabharwal, A.; Schoenick, C.; and Tafjord, O. 2018. Think you have Solved Question Answering? Try ARC, the AI2 Reasoning Challenge. arXiv:1803.05457.

Frantar, E.; Ashkboos, S.; Hoefer, T.; and Alistarh, D. 2023. GPTQ: Accurate Post-Training Quantization for Generative Pre-trained Transformers. arXiv:2210.17323.

Grattafiori, A.; Dubey, A.; Jauhri, A.; Pandey, A.; Kadian, A.; Al-Dahle, A.; Letman, A.; Mathur, A.; Schelten, A.; Vaughan, A.; et al. 2024. The Llama 3 Herd of Models. arXiv:2407.21783.

Jacob, B.; Kligys, S.; Chen, B.; Zhu, M.; Tang, M.; Howard, A.; Adam, H.; and Kalenichenko, D. 2017. Quantization and Training of Neural Networks for Efficient Integer-Arithmetic-Only Inference. arXiv:1712.05877.

Krishnamoorthi, R. 2018. Quantizing deep convolutional networks for efficient inference: A whitepaper. arXiv:1806.08342.

Li, Y.; Yin, R.; Lee, D.; Xiao, S.; and Panda, P. 2025. GPTAQ: Efficient Finetuning-Free Quantization for Asymmetric Calibration. arXiv:2504.02692.

Lin, L.; Hu, X.; and Wan, X. 2025. NeUQI: Near-Optimal Uniform Quantization Parameter Initialization. arXiv:2505.17595.

Merity, S.; Xiong, C.; Bradbury, J.; and Socher, R. 2017. Pointer Sentinel Mixture Models. In *International Conference on Learning Representations*.

Nair, P. A.; and Suggala, A. S. 2024. CDQuant: Greedy Coordinate Descent for Accurate LLM Quantization. arXiv:2406.17542.

Raffel, C.; Shazeer, N.; Roberts, A.; Lee, K.; Narang, S.; Matena, M.; Zhou, Y.; Li, W.; and Liu, P. J. 2020. Exploring the limits of transfer learning with a unified text-to-text transformer. *Journal of machine learning research*, 21(140): 1–67.

Sakaguchi, K.; Bras, R. L.; Bhagavatula, C.; and Choi, Y. 2021. Winogrande: An adversarial winograd schema challenge at scale. *Communications of the ACM*, 64(9): 99–106.

Touvron, H.; Martin, L.; Stone, K.; Albert, P.; Almahairi, A.; Babaei, Y.; Bashlykov, N.; Batra, S.; Bhargava, P.; Bhosale, S.; et al. 2023. Llama 2: Open Foundation and Fine-Tuned Chat Models. arXiv:2307.09288.

Xiao, G.; Lin, J.; Seznec, M.; Wu, H.; Demouth, J.; and Han, S. 2023. Smoothquant: Accurate and efficient post-training quantization for large language models. In *International Conference on Machine Learning*, 38087–38099. PMLR.

Yang, A.; Li, A.; Yang, B.; Zhang, B.; Hui, B.; Zheng, B.; Yu, B.; Gao, C.; Huang, C.; Lv, C.; et al. 2025. Qwen3 Technical Report. arXiv:2505.09388.

Zellers, R.; Holtzman, A.; Bisk, Y.; Farhadi, A.; and Choi, Y. 2019. HellaSwag: Can a Machine Really Finish Your Sentence? In Korhonen, A.; Traum, D.; and Márquez, L., eds., *Proceedings of the 57th Annual Meeting of the Association for Computational Linguistics*, 4791–4800. Florence, Italy: Association for Computational Linguistics.

Zhang, A.; Wang, N.; Deng, Y.; Li, X.; Yang, Z.; and Yin, P. 2024. MagR: Weight Magnitude Reduction for Enhancing Post-Training Quantization. arXiv:2406.00800.

Zhang, S.; Zhang, H.; Colbert, I.; and Saab, R. 2025. Qronos: Correcting the Past by Shaping the Future... in Post-Training Quantization. arXiv:2505.11695.

Zhu, X.; Li, J.; Liu, Y.; Ma, C.; and Wang, W. 2024. A Survey on Model Compression for Large Language Models. *Transactions of the Association for Computational Linguistics*, 12: 1556–1577.

## A Proofs

### A.1 General Form

**Lemma 1.** *If  $X^\top X$  is invertible, then*

$$\arg \min_Q \|XQ - Y\|_F^2 = \arg \min_Q \|X(Q - Q^*)\|_F^2, \quad (13)$$

where

$$Q^* = (X^\top X)^{-1} X^\top Y. \quad (14)$$

*Proof.* Consider the functions

$$f(Q) = \|XQ - Y\|_F^2, \quad (15)$$

$$g(Q) = \|X(Q - Q^*)\|_F^2. \quad (16)$$

We will demonstrate that  $f$  and  $g$  have identical gradients with respect to  $Q$ , and hence share the same minimizer.

First, expand  $f(Q)$  in trace form:

$$f(Q) = \text{tr}((XQ - Y)(XQ - Y)^\top) \quad (17)$$

$$= \text{tr}(Q^\top X^\top XQ) - 2 \text{tr}(Q^\top X^\top Y) + \text{tr}(Y^\top Y). \quad (18)$$

Differentiating with respect to  $Q$  gives

$$\nabla_Q f(Q) = 2X^\top XQ - 2X^\top Y = 2X^\top X(Q - Q^*). \quad (19)$$

Next, express  $g(Q)$  in trace form:

$$g(Q) = \text{tr}((Q - Q^*)^\top X^\top X(Q - Q^*)). \quad (20)$$

Its derivative is

$$\nabla_Q g(Q) = 2X^\top X(Q - Q^*). \quad (21)$$

Since  $\nabla_Q f(Q) = \nabla_Q g(Q)$  for all  $Q$ , the functions  $f$  and  $g$  differ only by a constant and consequently have the same minimizer. Therefore,

$$\arg \min_Q f(Q) = \arg \min_Q g(Q). \quad (22)$$

□

## A.2 Specific Form

In the methodology section, we aim to prove the following results, where we omit the subscript  $Q$  in  $\arg \min_Q$ :

$$\arg \min \|\hat{X}Q - XW\|_F^2 \quad (23)$$

$$= \arg \min \|\hat{X}(Q - (\hat{X}^T \hat{X})^{-1}(\hat{X}^T X)W)\|_F^2 \quad (24)$$

$$= \arg \min \|\hat{X}(Q - H^{-1}(H + C)W)\|_F^2 \quad (25)$$

$$= \arg \min \|\hat{X}(Q - (I + H^{-1}C)W)\|_F^2 \quad (26)$$

$$\arg \min \|(\hat{h} + \hat{X}Q) - (h + XW)\|_F^2 \quad (27)$$

$$= \arg \min \|\hat{X}Q - (XW + h - \hat{h})\|_F^2 \quad (28)$$

$$\begin{aligned} &= \arg \min \|\hat{X}(Q - ((\hat{X}^T \hat{X})^{-1}(\hat{X}^T X)W \\ &\quad + (\hat{X}^T \hat{X})^{-1} \hat{X}^T (h - \hat{h})))\|_F^2 \quad (29) \end{aligned}$$

$$\begin{aligned} &= \arg \min \|\hat{X}(Q - ((I + H^{-1}C)W \\ &\quad + H^{-1} \hat{X}^T (h - \hat{h})))\|_F^2 \quad (30) \end{aligned}$$

## B Quantization Techniques

In this section, we briefly introduce the quantization techniques involved in the Experiment section.

### B.1 GPTQ

Follow LDLQ proposed by QuIP, we revisit GPTQ and propose a more effective derivation approach, which can be formally expressed as follows.

$$\begin{aligned} \|\hat{X}(Q - W)\|_F^2 &= \text{tr}((Q - W)^\top (\hat{X}^\top \hat{X})(Q - W)) \\ &= \text{tr}((Q - W)^\top H(Q - W)) \\ &= \text{tr}((Q - W)^\top L^\top L(Q - W)) \\ &= \|L(Q - W)\|_F^2, \end{aligned} \quad (31)$$

where  $L$  is the Cholesky factor of  $H$  and is a lower triangular matrix. The term  $\|L(Q - W)\|_F^2$  can be decomposed into the sum of squared errors of each row. Notably, the  $i$ -th row of  $L(Q - W)$  is a linear combination of the first  $i$  rows of  $Q - W$ . This property enables sequential row-wise quantization. Consequently, we derive

$$Q = \text{Quant}(W - D^{-1}(L - D)(Q - W)), \quad (32)$$

where  $D$  denotes the diagonal matrix formed by the diagonal elements of  $L$ , and  $\text{Quant}(\cdot)$  maps each item to the nearest value in the quantization grid.

To ensure that  $H$  is positive definite, a sufficiently large term  $\lambda I$  is typically added. This is essentially equivalent to solving

$$\arg \min_Q \|\hat{X}(Q - W)\|_F^2 + \lambda \|Q - W\|_F^2. \quad (33)$$

Additionally, we follows the GPTQ heuristic of reordering each row based on the diagonal values of  $H$  in descending order.

### B.2 Hadamard transform

The Hadamard transform<sup>1</sup>, which is used in methods such as QuaRot and QuIP#, smooths the distributions of activations and weights, enabling more effective quantization while maintaining high efficiency due to the special structure of the Hadamard matrix, which allows fast computation. Specifically, it employs an orthogonal matrix  $R$  with entries  $\pm 1$ , enabling the transformations  $X' = XR$  and  $W' = R^{-1}W$ . Here,  $X'$  and  $W'$  serve as the transformed activations and weights that are subsequently used for quantization. When the transform is applied to a vector of length  $n$ , the computational complexity is  $O(n \log n)$  on a single worker and can be reduced to  $O(\log n)$  with sufficient workers.

### B.3 NeUQI

NeUQI is a quantization parameter initialization method designed for uniform quantization. It overcomes the limitations of the conventional Min-Max framework, particularly the restriction that the zero-point must be an integer, resulting in a highly efficient initialization method with significant performance improvements.

## C Implementation Details

### C.1 LoaQ Pipeline

The following algorithm describes the overall LoaQ pipeline.

<sup>1</sup>See [https://en.wikipedia.org/wiki/Hadamard\\_matrix](https://en.wikipedia.org/wiki/Hadamard_matrix)

---

**Algorithm 1: LoaQ Pipeline**


---

**Require:** Weights  $\{W_{\text{in}}^{(\ell)}, W_{\text{out}}^{(\ell)}\}_{\ell=1}^L$ , calibration inputs  $\{I^{(i)}\}_{i=1}^S$ , bit-width  $k$ , adjustment parameters  $\alpha, \beta \in [0, 1]$

**Ensure:** Quantized weights  $\{Q^{(\ell)}\}_{\ell=1}^L$

- 1: Run forward to collect embedding outputs  $h, \hat{h}$
- 2: **for**  $\ell = 1$  to  $L$  **do**
- 3:   **for**  $W$  in  $\{W_{\text{in}}^{(\ell)}, W_{\text{out}}^{(\ell)}\}$  **do**
- 4:     Run forward to collect activation  $X, \hat{X}$
- 5:     **if**  $W = W_{\text{in}}^{(\ell)}$  **then** ▷ quantize  $W_{\text{in}}$
- 6:        $H \leftarrow \hat{X}^\top \hat{X}$
- 7:        $C \leftarrow \hat{X}^\top (X - \hat{X})$
- 8:        $\Delta = \mathbf{0}$
- 9:     **else** ▷ quantize  $W_{\text{out}}$
- 10:        $s \leftarrow R(h + XW)$
- 11:        $\hat{s} \leftarrow R(h + \hat{X}W)$  ▷ Rescale for each token
- 12:        $X' \leftarrow sX$
- 13:        $\hat{X}' \leftarrow \hat{s}\hat{X}$
- 14:        $H \leftarrow \hat{X}'^\top \hat{X}'$
- 15:        $C \leftarrow \hat{X}'^\top (X' - \hat{X}')$
- 16:        $\Delta \leftarrow H^{-1} \hat{X}'^\top (sh - \hat{s}\hat{h})$
- 17:     **end if**
- 18:      $\widetilde{W} \leftarrow (I + \alpha H^{-1} C)W + \beta \Delta$
- 19:     Quantize:  $Q \leftarrow \text{QuantMethod}(\widetilde{W}; H; k)$
- 20:   **end for**
- 21:   Run forward to get updated sub-layer outputs  $h, \hat{h}$
- 22: **end for**
- 23: **return**  $\{Q^{(\ell)}\}_{\ell=1}^L$

---

## C.2 Hyperparameter

We perform a hyperparameter grid search by first tuning  $\alpha$  and then tuning  $\beta$ . Specifically,  $\alpha$  ranges from 0 to 1 in increments of 0.1 and  $\beta$  ranges from 0 to 1 in increments of 0.05.

$$\alpha \in \{0.1 \times i \mid i = 0, 1, 2, \dots, 10\}, \quad (34)$$

$$\beta \in \{0.05 \times j \mid j = 0, 1, 2, \dots, 20\}. \quad (35)$$

## D Supplementary Results

This appendix presents supplementary quantization results. Detailed results on 3-bit channel-wise quantization for LLaMA and Qwen families are shown in Table 7.

Model	Size	Method	Wiki2↓	C4↓	ArcC↑	ArcE↑	HellaS↑	PiQA↑	WinoG↑	Acc↑
7B	7B	GPTQ	8.39	9.98	33.02	65.15	48.98	73.50	63.77	56.89
		GPTAQ	7.61	9.15	34.81	68.52	50.06	74.32	<b>65.98</b>	58.74
		Qronos	7.80	9.17	33.45	67.26	50.19	74.05	64.25	57.84
		LoaQ	<b>7.46</b>	<b>8.92</b>	<b>39.51</b>	<b>71.13</b>	<b>51.57</b>	<b>75.41</b>	65.27	<b>60.58</b>
LLaMA 2	13B	GPTQ	6.45	8.00	<b>41.81</b>	73.82	55.08	76.44	68.27	63.08
		GPTAQ	6.31	7.84	40.96	<b>75.29</b>	55.30	76.66	<b>69.93</b>	<b>63.63</b>
		Qronos	6.39	7.88	41.04	74.96	54.50	76.12	69.69	63.26
		LoaQ	<b>6.26</b>	<b>7.76</b>	41.21	74.96	<b>55.47</b>	<b>77.48</b>	68.90	63.60
70B	70B	GPTQ	4.84	6.58	49.40	<b>80.72</b>	<b>60.80</b>	79.54	74.43	68.98
		GPTAQ	4.81	6.58	47.70	79.42	58.23	79.76	<b>74.59</b>	67.94
		Qronos	4.80	6.52	49.83	79.84	60.79	79.98	74.51	<b>68.99</b>
		LoaQ	<b>4.77</b>	<b>6.51</b>	<b>50.17</b>	79.38	59.95	<b>80.63</b>	74.43	68.91
LLaMA 3	8B	GPTQ	24.52	22.75	27.22	51.14	44.27	64.74	59.43	49.36
		GPTAQ	17.79	18.05	32.59	62.04	46.69	69.59	64.88	55.16
		Qronos	33.17	23.76	28.50	56.02	47.88	69.64	63.69	53.15
		LoaQ	<b>12.53</b>	<b>15.01</b>	<b>32.85</b>	<b>63.38</b>	<b>50.23</b>	<b>73.45</b>	<b>66.38</b>	<b>57.26</b>
70B	70B	GPTQ	<b>1909</b>	<b>931</b>	20.90	25.21	<b>26.15</b>	52.50	51.38	35.23
		GPTAQ	>1e4	8500	20.39	<b>25.67</b>	25.70	<b>53.10</b>	50.51	35.08
		Qronos	>1e4	7331	20.90	25.08	25.85	52.61	51.07	35.10
		LoaQ	>1e4	>1e4	<b>22.35</b>	24.75	25.82	52.99	<b>51.78</b>	<b>35.54</b>
8B	8B	GPTQ	14.74	17.36	32.59	52.69	47.97	71.55	56.51	52.26
		GPTAQ	14.03	16.77	37.37	66.84	48.45	72.63	61.64	57.39
		Qronos	14.21	16.69	38.74	65.91	48.62	71.55	62.83	57.53
		LoaQ	<b>13.72</b>	<b>16.68</b>	<b>41.55</b>	<b>74.24</b>	<b>49.50</b>	<b>74.32</b>	<b>64.88</b>	<b>60.90</b>
Qwen 3	14B	GPTQ	12.43	14.88	43.52	71.46	53.19	75.14	63.85	61.43
		GPTAQ	<b>11.78</b>	14.73	45.90	74.28	53.29	76.06	68.43	63.59
		Qronos	12.06	14.75	<b>47.18</b>	<b>76.89</b>	53.74	<b>76.66</b>	67.40	<b>64.38</b>
		LoaQ	11.86	<b>14.70</b>	46.25	75.72	<b>54.47</b>	75.79	<b>68.90</b>	64.22
32B	32B	GPTQ	11.71	14.06	40.87	67.09	55.95	74.92	62.59	60.28
		GPTAQ	10.87	13.44	<b>48.29</b>	74.45	56.87	75.95	67.80	64.67
		Qronos	11.32	13.52	44.45	73.19	56.76	<b>76.99</b>	68.43	63.96
		LoaQ	<b>10.56</b>	<b>13.10</b>	45.56	<b>75.25</b>	<b>57.58</b>	76.88	<b>69.69</b>	<b>64.99</b>

Table 7: Results of 3-bit channel-wise quantization, applied to the LLaMA 2, LLaMA 3, and Qwen 3 model families.